Iranian Journal of Medical Physics
Vol. 13, No. 4, December 2016, 236-249
Received: July 30, 2016; Accepted: September 24, 2016

Original Article

Estimation of Secondary Skin Cancer Risk Due To Electron Contamination in 18-MV LINAC-Based Prostate Radiotherapy

Seyed Mostafa Ghavami[1], Hosein Ghiasi[2*]

Abstract

Introduction
Accurate estimation of the skin-absorbed dose in external radiation therapy is essential to estimating the probability of secondary carcinogenesis induction
Materials and Methods
Electron contamination in prostate radiotherapy was investigated using the Monte Carlo (MC) code calculation. In addition, field size dependence of the skin dose was assessed. Excess cancer risk induced by electron contamination was determined for the skin, surface dose, and prostate dose-volume histogram (DVH) using MC calculation and analytical methods.
Results
MC calculations indicated that up to 80% of total electron contamination fluence was produced in the linear accelerator. At 5 mm below the skin surface, surface dose was estimated at 6%, 13%, 27%, and 38% for 5×5 cm^2, 10×10 cm^2, 20×20 cm^2, and 40×40 cm^2 field sizes, respectively. Relative dose at D_{max} was calculated at 0.92% and 5.42% of the maximum dose for 5×5 cm^2 and 40×40 cm^2 field sizes, respectively. Excess absolute skin cancer risk was obtained at 2.96×10^{-4} $(PY)^{-1}$ for total 72 Gy. Differences in prostate and skin DVHs were 1.01% and 1.38%, respectively.
Conclusion
According to the results of this study, non-negligible doses are absorbed from contaminant electrons by the skin, which is associated with an excess risk of cancer induction.

Keywords: Skin Cancer, Monte Carlo Method, High Energy Radiotherapy, Absolute Risk Reduction, Prostate Cancer, Radiotherapy

1-Department of Radiology, Paramedical School, Tabriz University of Medical Sciences, Tabriz, Iran
2- Medical Radiation Sciences Research Team, Tabriz University of Medical Sciences Tabriz, Iran.

*Corresponding author: Tel: +984137792565; Fax: +984137792564; E-mail: hoseinghiasi62@gmail.com

1. Introduction

Radiation therapy is performed on more than half of all cancer patients in developed countries [1]. Although radiation therapy is associated with undesirable side effects, use of conservative, accurate techniques could significantly reduce such complications. Metaphorically, radiation resembles a double-edged knife, and incautious conduction of radiation therapy may cause irreversible damage to normal tissues.

Despite the benefits of radiation therapy in tumor control and disease palliation, it is likely to pose risk to normal tissues if the process is delivered without the necessary caution and protection. Primarily, radiotherapy aims to maximize irradiation benefits and minimize undesirable complications. Poor treatment plans in this regard might expose the normal organs of patients to inaccurate radiation doses and cause radiation contamination, which is associated with various health complications, such as secondary-induced malignancies [2-5].

Radiation-induced secondary malignancies may be considered as a penalty for cancer treatment, the utmost control of which is of paramount importance. Secondary malignancies and radiation-induced carcinogenesis occur mainly due to radiation contamination and out-of-field radiation. Secondary cancer is defined as the histologically distinct cancer that develops following the first cancer treatment, one of the most notable properties of which is the presence of a latency period.

Secondary cancers induced by radiotherapy have various characteristics. For instance, diagnosis of these cancers is possible after a latency period following radiation therapy, while these cancer types histologically differ from the primary cancerous tissues. In this regard, the latency period has been reported to last more than five years [6].

Most non-melanoma skin cancers account for basal or squamous cell carcinomas, which are the most prevalent cancers of skin tissues. Since they rarely spread to normal organs or sites in the body, basal and squamous cell carcinomas involving the skin cells are usually less alarming and treated differently than melanoma.

According to statistics, second malignant neoplasms and cardiovascular diseases are the most frequent adverse events associated with radiotherapy.

Another example of secondary complications in this regard is the increased risk of solid cancers after radiotherapy for Hodgkin's lymphoma [7]. Additionally, risk of secondary cancers has been reported to be 15.5 per 10^3 person-years (PY^{-1}) in prostate, lung, colorectal and ovarian radiotherapy [6].

In a study, Haung et al. [8] compared 2,120 cancer patients receiving radiation therapy with 2,120 cancer patients undergoing surgery, reporting a significant incidence rate for secondary cancers in radiation therapy patients.

Furthermore, in a detailed study conducted in this regard, a five-fold increase was observed in the rate of secondary cancers after a 10-year follow-up in patients receiving radiation therapy. Another research by Murray L et al. proposed further detailed data on the risk of secondary cancers following radiotherapy [6].

Skin cancers are considered as one of the most prevalent complications associated with radiotherapy, commonly classified as melanoma and non-melanoma. Non-melanoma skin cancers are of two types, including basal cell carcinoma (BCC) and squamous cell carcinoma (SCC). Despite its higher frequency, BCC is rarely fatal, while it may lead to disfigurement in many cases. Skin toxicity is another complication associated with radiotherapy, which adversely affects the quality and different aspects of patient care [7].

Extensive research has been conducted regarding radiation contamination. For instance, Bilge et al. [9] measured the surface dose for 6-MV and 18-MV photon beams using GafChromic film. According to the findings, surface dose was within the range of 15-39% of D_{max} for 6-MV beams, while it was 6-32% of D_{max} for 18-MV linear accelerator (LINAC) photon beams in 5×5 cm^2, 10×10 cm^2, 20×20 cm^2, and 30×30 cm^2 filed sizes. Therefore, it was concluded that increased field size is associated with a higher surface dose due to extra electron contamination and head-scattered photons.

In the mentioned study, maximum dose at the phantom surface was observed in the field size of 30×30 cm^2, with the 6-MV photon beam of 40%. On the other hand, minimum surface dose was obtained at 6% of D_{max} dosein the field size of 5×5 cm^2 with 18-MV photon beam prostate radiotherapy.

In another research, Butson et al. [10] investigated the surface dose of radiation contamination in a phantom. According to their findings, doses of electron contamination at 0.05-mm depth (basal cell layer) were 65% and 90%, while they were 52% and 79% at 1-mm depth (dermal layer), and 15% and 26% at 10-mm depth (subcutaneous tissue) in 10×10 cm^2 and 40×40 cm^2 field sizes, respectively.

In the mentioned study, measurements were performed using a Varian 2100C LINAC operating at 18-MV photon mode. Obtained results indicated the position of the maximum electron contamination dose to be at the depth of 32-40 mm from the phantom surface, where the percentage dose of contaminant electrons was 6%±2% of the maximum dose. Finally, it was concluded that the main surface dose (approximately 90%) was closely correlated with the contaminant electrons in largest field size (40×40 cm^2). It is also noteworthy that the value dropped to 67% in a smaller field size (10×10 cm^2).

According to the findings of Zhu and Palta [11], electron contamination at the surface was 1-33% and 2-44% of the maximum dose for 8-MV and 18-MV photon beams, respectively. Furthermore, contaminant dose percentage was determined independently of the source-to-surface distance (SSD), and reduction of depth was reported as well.

In this regard, extensive studies could be found in the current literature [12-17]. Considering the low penetration and high absorption of electrons in superficial tissues, the skin absorbs most of the received contaminant electrons from the LINAC head assembly and air. This may lead to the occurrence of secondary malignancies in skin surface tissues.

Proper management of cancer patients and prevention of malignancy recurrence requires the sufficient delivery of the prescribed radiation doses to the target organ. Therefore, an accurate knowledge of the skin dose and received dose by the target organ is of paramount importance. In this respect, the skin-absorbed dose must be lower than its radiation tolerance during the delivery of the dose into deeper organs. In a study, Trott and Kummermehr [18] reported that induced early reaction develops within the range of 30-40 Gy and 2-Gy fractions.

In another research by Lewanda et al. [19], epilation was observed in after 50% of total doses delivery in the range of 40 Gy in 2-Gy fractions. Moreover, tolerance dose for permanent epilation was reported to be in the range of 10 Gy. The researchers stated that irreversible effects may develop at doses above 50 Gy in the sweat and subcutaneous glands.

This study aimed to investigate and calculate the dose of electron contamination and determine its characteristics. Additionally, we estimated the risk of secondary skin cancer due to electron contamination in prostate radiotherapy.

Several studies have focused on secondary cancer risk estimation following radiation therapy. For instance, Schneider [20] and Hall and Wuu [21] proposed the cell-kill model and flat dose-response model as the analytical methods for the estimation of secondary cancer incidence, respectively. These models presented the risk of cancer incidence based on the competition between cell survival and induction of DNA mutations as two biological effects.

This study aimed to characterize the electron contamination and its carcinogenesis effects using the Monte Carlo (MC) simulation and mathematical model-based calculation. Furthermore, a four-field box prostate radiotherapy plan was considered and modeled by the MC method. Dose-volume histogram (DVH) for prostate tumors and skin (as the normal tissue) was obtained by the treatment planning system (TPS) data and MC simulation for the comparison of the results.

2. Materials and Methods

For the simulations and calculations in this study, we used the Monte Carlo N-Particle Transport code $MCNP_X$ version 2.6.0, which has been recently released by the Los Alamos

National Library (LANL). The code consists of the features and capabilities to increase its ability for complex geometric simulations and rapid problem solving. The main parts of the head of 18-MV Varian 2100C LINAC were simulated in accordance with the guidelines of the manufacturer. These parts included primary electrons, target, electron stopper, bending magnet, primary and secondary collimators, flattening filter, mirror, movable jaws and a massive head shielding. Simulated model was validated and verified through comparison with MC-derived percent depth dose (PDD) and beam profile (BP) data in different field sizes.

Differences up to 2% in the lateral regions of BP and 0.98% in D_{max} of PDD curves were obtained based on the MC-derived data and direct measurement in all the studied field sizes. Derived PDD and BP datasets by direct measurement and MC simulation are depicted in figures 1.a and 1.b.

A standard adult male phantom (ORNL mathematical-based phantom) with a small prostate gland tumor was modeled as the patient. While running the program, optimaum bremsstrahlung X-ray production was calculated and BNUM value was changed in the data card of the program (PHYS: E).

Setting the BNUM value as five, the code produced five photons per initial incident electron, and simultaneously followed five photons history per initial electron.

To optimize the BNUM value in the data card, we increased the speed and reduced the run time by four times. Four-field-box (FFB) technique was considered as the treatment plan to deliver the prescribed radiation dose to the malignant site of the prostate.

Contaminant electron spectra generated by the modeled LINAC head was calculated at the surface. Moreover, air-generated and total electron contamination was estimated, as well as the head-produced electron contamination components. Due to the low penetration of electrons into the tissue, we only calculated the skin-absorbed dose of contaminant electrons, and the secondary skin cancer incidence risk was estimated in two field sizes of 8×8 cm^2 and two 8×7 cm^2.

Secondary cancer risk estimation was carried out in accordance with the guidelines of the International Commission on Radiological Protection (ICRP) (Report No. 103) [21]. In addition, dose equivalent and effective dose were calculated based on the data and formulations of ICRP. In total, 72 Gy dose deliveries were considered in 36 fractions using the FFB technique for the prostate tumor, and secondary cancer risk was estimated through the formulation of analytical models based on the calculated skin dose absorbed from electron contamination. For cancer risk estimation, total electron dose equivalent to skin was obtained based on the MC code calculation.

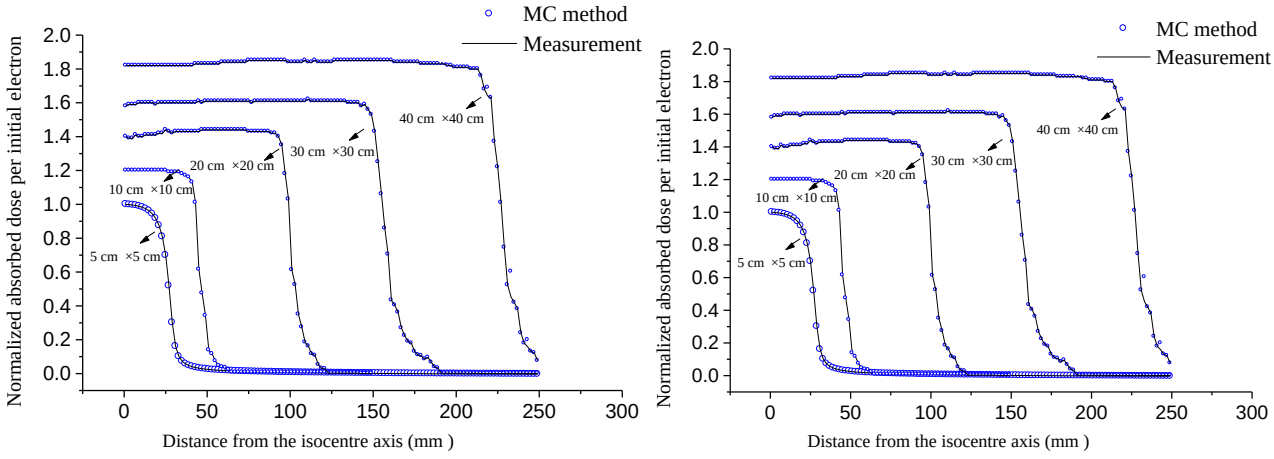

Figure 1. a) Normalized BP derived by MC simulation and measurements data in different field sizes.b) Normalized PDD derived by MC simulation and measurements data in different field sizes.

In this study, the formulated analytical models for secondary cancer risk estimation in radiation therapy were acquired through empirical observations or based on theories. Furthermore, we evaluated the analytical models proposed by Schneider et al. [20] and Hall and Wuu [21], which were applied to demonstrate the competing effects of cell survival and DNA mutations on cells.

As described by Schneider et al. [20], risk of radiocarcinogenesis to an organ is signified by T in equation one, as follows:

$$R_T = \sum_T f_{T,low} \times S_T \times H_T \quad (1)$$

Where $f_{T,low}$ is the excess absolute risk per unit dose (10^4 per year per Gy) at low doses, S_T denotes an exponential parameter ($e^{-\alpha_T \times H_T}$), and H_T represents the tissue dose equivalent (Sv. effective dose). *Effect* (D_i) is the dose that, if administered uniformly to the entire volume, leads to the same normal tissue complication probability (NTCP) as the non-uniform dose distribution.

Poisson model for $P(D_i)$ is used in TPSs for NTCP calculation, which is presented in equation 4. In this equation, TD_{50} signifies the uniform dose received by the whole organ causing a 50% risk of complications, and D_i represents the total equivalent 2-Gy fraction doses. Additionally, α_T in S_T (exponential phrase) is in Gy^{-1}, considering the cell-kill parameter in risk estimation (R_T), which is reported in 10^4 $(PY)^{-1}$.

DVHs for the prostate tumor and skin were calculated using the MC method, and TPS- and MC-derived DVHs were compared for the tumor and skin. By selecting the "body" in TPS, skin DVH was obtained. Total volume of the organs (prostate and skin) was equally divided into 20 parts (5% of total volume) based on the MC code, and subvolume doses were categorized using the MATLAB software.

To derive DVH, irradiated areas of the four aforementioned field sizes were summed up. Division of the volumes was performed using the MC code by inserting the required data into a written data card. Afterwards, the code created equal subvolumes automatically, and dose calculation was conducted for all the subvolumes. NTCP was calculated using equation two, as follows [21, 22]:

$$NTCP = \left[1 - \prod_{i=1}^{n} \left[1 - P(\lambda_i \times D_i)^s\right]^{\Delta v_i}\right]^{1/s} \quad (2)$$

Moreover, complication due to D_i was calculated using equation 3, as follows:

$$P(D_i) = 2^{-e\times\gamma^{(1-D_i/D_{50})}} \quad (3)$$

In NTCP description, λ_i was determined using equation four, as follows:

$$\lambda_i = \frac{\frac{\alpha}{\beta} + \frac{D_i}{N_{fr}}}{\frac{\alpha}{\beta} + D_{2Gy}} \quad (4)$$

As proposed by Kutcher, the NTCP model is used to determine the heterogeneous dose distribution. In this regard, λ_i, Δv_i (subvolume), D_i, and D_{50} are interpreted similar to the Lyman model for NTCP calculation.

γ is the normalized slope of the S-shaped dose-response curve, where the absolute dose response gradient is at its steepest. In addition, D_i signifies the total prescribed dose (72 Gy), N_{fr} represents the number of fractions (n=36), and D_{2Gy} is the fractionated dose. In this equation, α/β ratio shows radiation sensitivity as a key characteristic of the tissue.

In this study, equally divided subvolumes were obtained through the division of the total volume by 20 (for each field sizes) and 80 (four field sizes) in prostate FFB irradiation. This value was determined at 17.39 cm^3 by dividing the total irradiated skin volume into 80 equal sections. Additionally, the value was used to derive DVH by MC calculation.

In this study, $f_{T,low}$ value was set at 0.58 $(10^4$ $PY)^{-1}$, and α_T was determined at 0.047 Gy^{-1} for the excess absolute cancer risk estimation 10^4 $(PY)^{-1}$ per Gy of skin dose. DVH of the skin-irradiated volume was derived by MC and compared with the TPS value. To benchmark our modeling, DVH of electron contamination

dose for skin was derived, and the required parameters for NTCP calculation were obtained via inverse calculations using the BIOPLAN software. Finally, NTCP was calculated for the contaminant electrons of the skin.

3. Results

In this study, MC code calculation was performed to characterize the electron contamination and secondary cancer risk induction in skin tissues due to electron contamination in prostate irradiation. In the standard field size of 10×10 cm^2, 1.2×10^{-16} Gy was found to be the absorbed dose at D_{max} (3.5 cm for 18-MV photon beam based on both methods) from the LINAC-produced photon beam per initial electron. Differences between the two applied methods in the build-up region could be attributed to contaminant electrons and insufficient equilibrium.

According to our findings, 8.33×10^{15} primary electrons were required for 1-Gy dose absorption at D_{max}, and the same calculation was made for the other field sizes. Since the results in MC output file are represented as the "result per initial particle", this calculation was required for the conversion of the MC-estimated doses into Gy for all the field sizes (Table 1).

Result of the code calculation for the relative electron dose in different depths of the phantom in the simulated field sizes was shown in Table 1. According to the information in this table, larger field sizes received higher electron contamination through the skin tissue. In the 40×40 cm^2 field size, relative absorbed dose in 1-mm depth was 6.33 times higher than that of the 5×5 cm^2 field size. Furthermore, surface doses at 5 mm below the skin surface were calculated to be 6%, 13%, 27%, and 38% for 5×5 cm^2, 10×10 cm^2, 20×20 cm^2, and 40×40 cm^2 field sizes, respectively. However, relative dose at D_{max} was determined at 0.92% and 5.42% of the maximum dose for 5×5 cm^2 and 40×40 cm^2 field sizes, respectively.

Simulation of a tray in the LINAC geometry was observed to increase the relative dose of electron by up to 22% in the field size of 40×40 cm^2, while wedge insertion decreased the relative dose by 2.5% in the standard field size of 10×10 cm^2. Furthermore, by using an energy tally in the tally card of the simulation, mean energy of the photon beam and contaminant electron radiation was obtained at 4.74 and 3.62 MeV in the 10×10 cm^2 field size, respectively. These values were calculated to be 3.66 and 3.26 MeV in a larger field size (40×40 cm^2), respectively.

Table 1. Electron contamination dose in the different depths below the skin surface relative to isocentre dose in percent of the isocentre dose

Field Size =5×5 (cm^2)							
Depth (mm)	1	3	5	7	9	11	mean
Relative Dose (%)	6	4	3	2	2	2	3
Field Size =10×10 (cm^2)							
Depth (mm)	1	3	5	7	9	11	mean
Relative Dose (%)	13	9	8	6	5	5	7
Field Size =20×20 (cm^2)							
Depth (mm)	1	3	5	7	9	11	mean
Relative Dose (%)	27	23	16	13	11	10	16
Field Size =40×40 (cm^2)							
Depth (mm)	1	3	5	7	9	11	mean
Relative Dose (%)	38	35	26	22	21	21	27

According to the MC calculation, the head-generated electron contamination played the most critical role in total electron contamination. In 10×10 cm^2 and 40×40 cm^2 field sizes, approximately 80% of the electron contamination was generated in the LINAC head. It is also noteworthy that in our modeling, electron fluence increased to 11% at the isocenter due to the presence of air. Calculation of the head-generated electron contamination in the 10×10 cm^2 field size indicated that electron contamination was 4.3 times higher than the air-generated contamination. At D_{max}, relative dose of electron was determined at 0.92%, 2.30%, 4.15%, and 5.21% in field sizes of 5×5 cm^2, 10×10 cm^2, 20×20 cm^2, and 40×40 cm^2, respectively. To calculate photon and electron fluence, ratio of contaminant electron fluence to photon beam fluence was obtained at 0.39% and 0.82% in field sizes of 10×10 cm^2 and 40×40 cm^2, respectively.

To insert a block into the photon beam pathway, relative surface dose was determined at 5.8-55%, which was obtained by increasing the field size from 5×5 cm^2 to 40×40 cm^2. Irradiated skin volume in the field was 1391.9 cm^3 with the prostate volume of 81.9 cm^3. Absorbed skin dose from the electron beam was calculated at 7.3%±1% Gy by the simulation, while the mean TPS was determined at 7.4 Gy.

Skin-absorbed dose from electron contamination was 10.27% of the prescribed dose to be delivered to the prostate (72 Gy). According to the results of MC simulation presented in Table 1, 28% of the prescribed dose was delivered to the skin at depth of 11 mm, 10% of which was due to electron contamination and 18% was absorbed from the photon beam. Applied field sizes in this regard were as follows: 8×8 cm^2 with SSD of 92.1 cm, 8×8 cm^2 with SSD of 92.5 cm, 7×8 cm^2 with SSD of 84 cm, and 7×8 cm^2 with SSD of 84.9 cm. Radiation treatment planning using the CorePlan TPS, including the irradiation fields, is depicted in Figure 2. Value of the attenuation factor for contaminant electrons was obtained at 0.81-1.19 cm^{-1} from the simulated 18-MV photon beam of Varian 2100C LINAC. Although the spectrum of contaminant electrons was smaller in altitude compared to that of the photons, shapes of the photon and electron spectra were similar on the skin surface.

Dose-dependency is not the only factor involved in the biological effectiveness of radiation therapy. Rate of the received dose plays a pivotal role in the management of intracellular damages and the repair process. In addition to dose-dependency and dose rate, ICRP publication 103 proposes another parameter to be involved in malignancy risk estimation due to radiation therapy [21]. Accordingly, a judged factor, generalizes the usually lower biological effectiveness (per unit of dose) of radiation exposures at low doses and low dose rates as compared with exposures at high doses and high dose rates. Photons are known to have a higher dose rate, while contaminant electrons have been shown to have a very low dose rate. It is noteworthy that this factor is tissue-dependent, and cell characteristics (α and β) of a specific tissue should also be considered in this regard.

By definition, value of the mentioned factor increases at low α/β ratios. In this study, effects of α/β factor on the skin were determined through applying the radiological characteristics of the skin tissue (α and β) and insertion of the calculated dose equivalent in the analytical model (Figure 3). Moreover, considering the factor defined by ICRP [21] and using analytical models, variable effects of the dose and dose rate on excess cancer risk were investigated in this study. According to our findings, these effects significantly declined with reduced dose rate and increased dose.

Variations in cancer risk with different dose and dose rates are illustrated in Figure 4. For the calculation of biological effects, we used a model consisting of two parts: the first term (in the figure 4 data calculations represented the DNA mutations caused by the radiation dose, and the exponential term indicated the cell survival variations associated with the absorbed radiation dose. The calculated effect using the analytical formulations is the competition result of the mentioned terms, in which cell survival decreases significantly due to the dominant effect of mutations in low-dose regions.

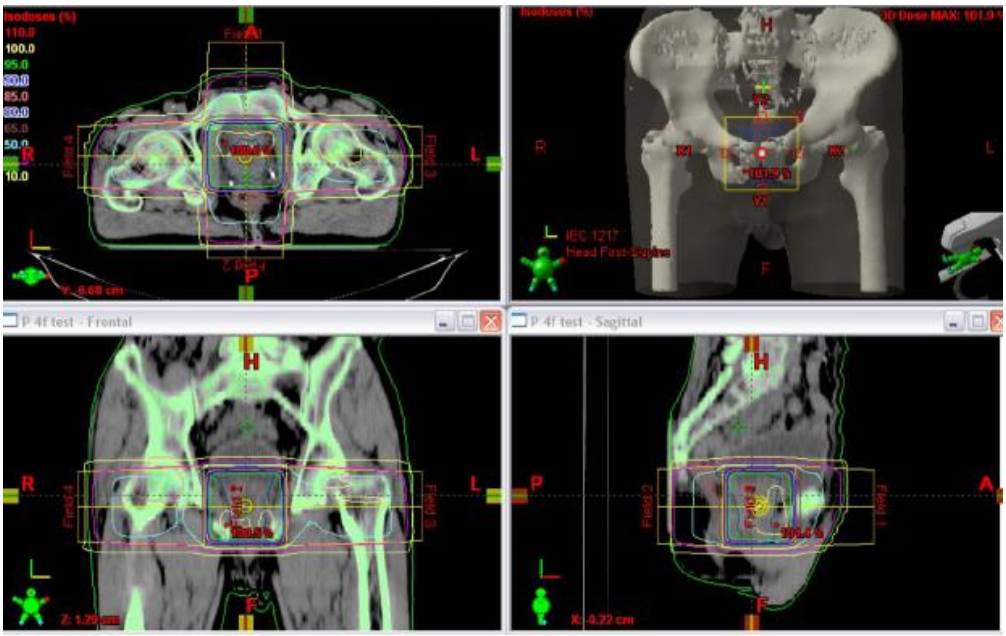

Figure 2. Core Plan TPS treatment planning for FFB irradiation of the prostate which shows isodoses in the patient body.

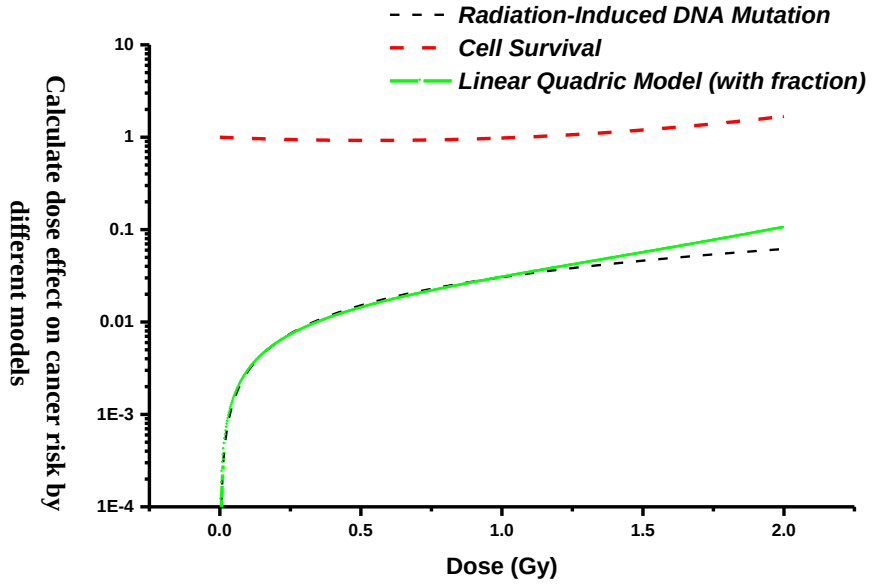

Figure 3. The proposed model calculated biological effect of the electron contamination on the skin. The effect is the result of competition of two parameters; cell survival and DNA mutation.

With the received fractionated dose of 7.4 Gy and "dose" and "dose rate" factors equal to one (as recommended for high doses), excess absolute risk for in-field skin was calculated to be 2.96×10^{-4} $(PY)^{-1}$Total dose from photon beams and electron contamination increased the risk of cancer since the electron dose was only a portion of the total surface dose (26% of total dose in 1-mm depth).

MC calculation in this study included the estimation of NTCP for skin tissues, and equations 1-4 were used for analytical measurements in this regard. Considering the volume of the skin tissue regions irradiated uniformly (by prostate four field box technique shown in figure 2), as reported in the literature, [23, 24, 25] .

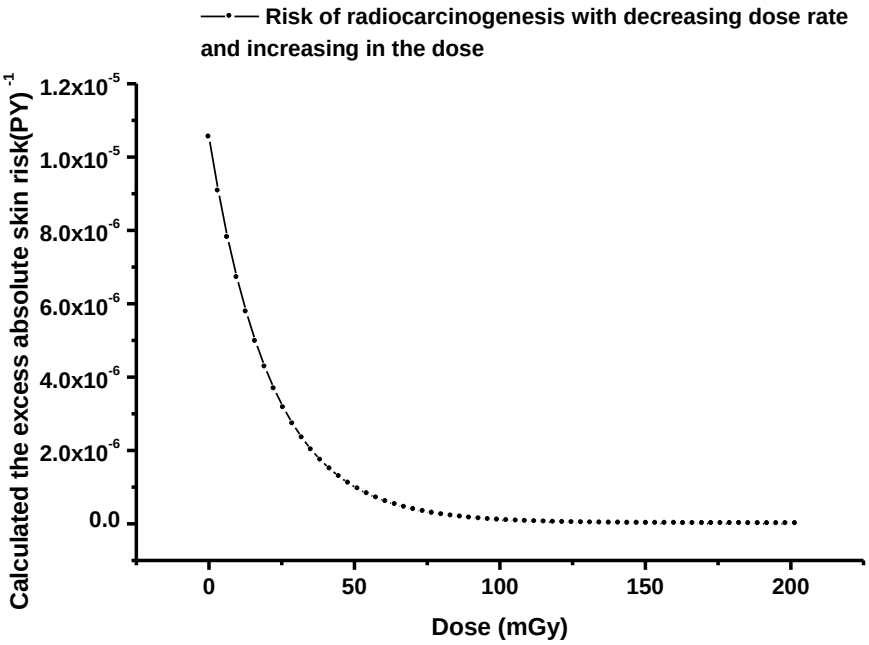

Figure 4. Calculated excess absolute cancer risk for the skin tissue while dose rate increases from 100mGy per hour to 0 and dose increases from 0 to 200mGy

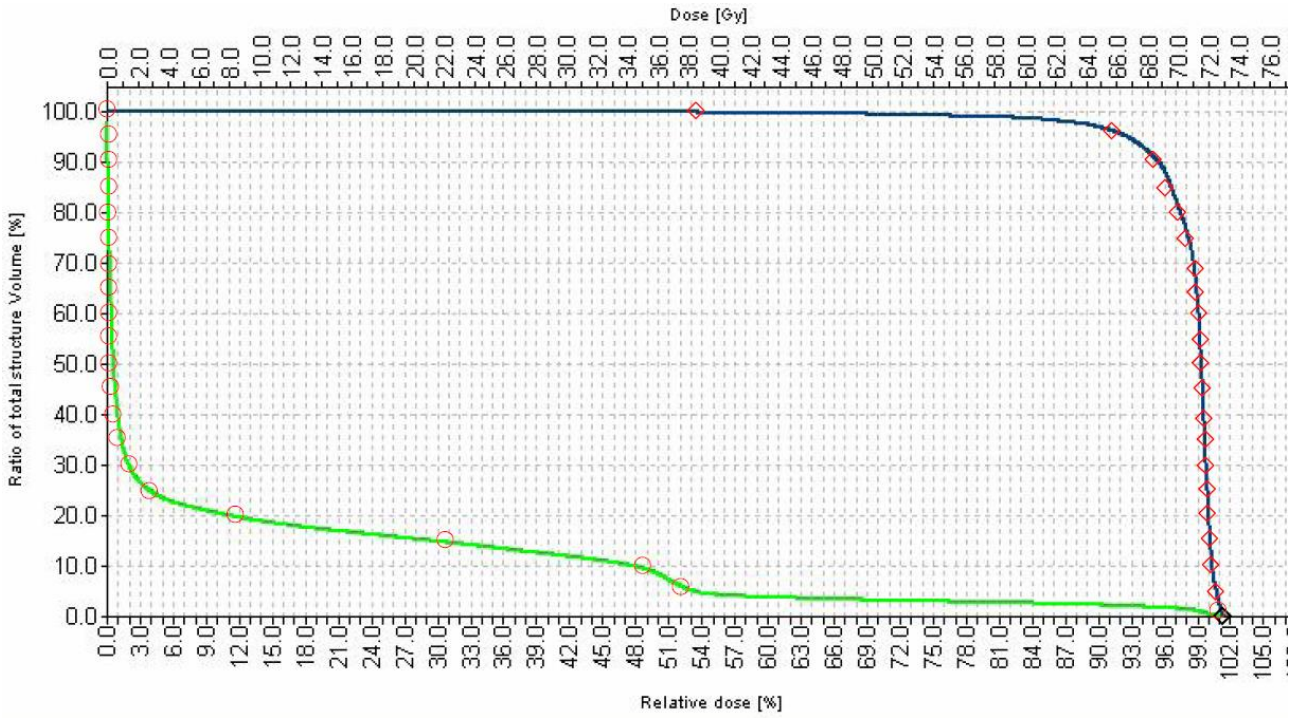

Fig. 5. CorePlan TPS derived and MC calculated DVHs for prostate and skin of patient. Solid lines show the TPS derived result and open marks (with 5% volume steps) show the MC calculation results.

NTCP value was calculated to be 14.65% for skin as the normal tissue in FFB treatment planning technique for prostate tumor. This finding was compatible with the utilized TPS-derived results determined at 14%. However, further investigation is required regarding the DVH of other TPSs.

In this study, skin was considered as the normal tissue, while prostate was considered as the tumoral tissue. Calculated DVHs for prostate and skin tissues are depicted in Figure 5. Utilized

TPS results and our MC modeling calculation were consistent. In the MC model, total volume of the prostate and skin was divided into 20 similar subvolumes in each field, and the absorbed doses were attributed to the related volume (5% of the total volume). It is noteworthy that higher precision of the results requires a larger number of volume intersections and longer MC duration in order for obtaining an acceptable statistical error. Our calculations were associated with a statistical error of less than 0.009 in all the subvolumes.

In the MC dose calculations to derive DVH, a higher difference with TPS-derived DVH was observed in the prostate (1.01%) and skin (1.38%). Further elaboration on the DVH calculation process has been presented in the Materials and Methods section. Results of DVH comparison benchmarked our model for electron DVH calculation. Moreover, based on the data from the BIOPLAN analysis of electron DVH, γ was obtained at 5.1 for the skin tissues irradiated by contaminant electrons.

Finally, skin NTCP due to electron contamination in prostate phototherapy by 18-MV LINAC and FFB technique was estimated as9%, while it was obtained as 15% for the total surface dose. It should be noted that this value increases by considering the dose of photoneutrons.

4. Discussion

The present study aimed to measure the electron contamination in an 18-MV Varian 2100C LINAC during prostate radiotherapy. Additionally, using the skin electron dose, secondary cancer induction risk was estimated for skin as the normal tissue. In the characterization of electron contamination, relative surface dose was calculated by MC simulation.

Several studies have investigated electron contamination and surface dose due to contaminant electrons in X-ray radiotherapy and radionuclide therapy. This could be due to the fact that at higher doses, cell killing exerts a dominant effect and mutation becomes negligible, while radiobiological effects are mainly deterministic. Furthermore, at high doses and dose rates, dominant cell survival effects represent the radiation effect better.

In a study, Zwicker et al. [26] assessed electron contamination due to Lucite in a 45-MV photon beam, reporting that the surface dose increased to 58% of the maximum dose. However, our simulation estimated the surface dose to rise by 38% of the maximum dose. This difference could be attributed to the variations in the energy of photon beams. Peak energy of the unit in the mentioned study was 2.5 times higher than the current research. High-energy photons produce more electrons in atom-photon interactions.

In another research in this regard, Li et al. [27] investigated electron contamination and its effect on PDD photon beam in the presence of a 0.1-cm lead leaf as filter, which reduced the surface dose from contaminant electrons by more than 95% for megavoltage beams from the ^{60}Co beam quality to 50-MV photon beam. Moreover, the researchers claimed that by using the 0.1-cm lead filter, only the photon dose participated in the surface dose, limiting the surface dose from contaminant electrons.

Similarly, Mallikarjuna et al. [28] reported lead to be an effective filter for field sizes as large as 30×30 cm^2 and 10-MV LINACs. In the mentioned research, three 10-MV LINACs with clear lead filters were examined, and no significant differences were reported, with the exception of the D_{max} location between the accelerators. Furthermore, Smit and Plessis [29] conducted an investigation in this regard and reported higher surface dose percentages with increased field size. These findings are in congruence with the results of the present study.

According to the results obtained by Smit and Plessis [29], electron contamination weight at the maximum dose in 15-MV photon beam was 0.4%, while this value was 1% higher, in our research compared to the mentioned study for the 18-MV beam. This difference could be attributed to the energy and LINAC head alloys. Since the head-generated contaminant electrons constitute approximately 80% of the

total electron contamination, any changes in the size of head components, materials and energy of LINAC might lead to non-negligible differences.

Findings of the present study regarding the effect of field size and weight of electron contamination in photon dose are consistent with the results obtained by Smit and Plessis [29]. On the other hand, results of the current research are in line with the study by Harper et al. in terms of the effect of field size and increased surface dose by inserting a block into the radiation field [30]. However, in the research by Harper et al., 4-MV and 10-MV LINACs were used, while the trend of variations in the surface dose was similar to our findings with the 18-MV LINAC. In another study by Nilsson and Brahme [31], cause of increased surface dose was reported to be the backward-scattered photons producing electrons in the phantom.

In their study, Mesbahi et al. [32] investigated the effect of a flattening filter (FF) on electron contamination, reporting that electron contamination decreased in the presence of FF. In addition, their findings were indicative of increased electron fluence (1.6 times) normalized to photon fluence in the absence of FF or flattening filter-free LINAC. These results are conceptually in line with the present study in terms of wedge insertion, which led to the reduction of electron fluence and surface dose.

In this regard, Sjogren and Karlsson [33] stated that the head-generated electrons had a dominant effect on the calculation of total electron contamination. This is consistent with the results of the current research, which showed that 80% of the total electron production was induced by the head-generated electrons.

With respect to surface dose, portion of electrons in D_{max} and electron contamination in different field sizes, our findings are in congruence with various studies [34-36]. In addition to similar modeling [28-36], this consistency confirms the validity of skin cancer estimation in our research.

MC-derived DVH in the present study was well adapted with the utilized TPS-derived DVH. Differences in skin DVHs derived by MC and TPS (up to 1.38%) might be due to the fact that TPSs are not able to calculate the surface dose accurately in contrast to deep doses. This confirms the accuracy of our modeling for precise calculations.

Although dose delivery from electron contamination to patient's skin is unwanted, a method has been proposed to remove contaminant electrons without changing the tumor dose in X-ray phototherapy. In this approach, a magnetic field is established by a device, decreasing up to 70% of basal cell electron dose, which significantly reduces carcinogenesis in skin tissues [37].

In terms of MC-derived DVH, application of MC simulation to derive DVH and accuracy of treatment planning, our findings are in line with the results of previous studies in this regard [38, 39]. For instance, Rudvat et al. evaluated the effects of multiple prognostic factors on acute skin reaction, while comparing the impact of hypofractionation (HF) with conventional fractionation (CF), tangential beam intensity-modulated radiation therapy, and three-dimensional conformal radiotherapy. According to the results, HF was associated with a more significant reduction in maximal acute skin reaction compared to CF [40].

In another study, Young DS et al. [41] assessed various personal, clinical and radiation-dosimetric parameters in breast radiotherapy for skin dose calculation. Moreover, scores of the intensity (range: 1-5) and extent of erythema (range: 0-1) were determined for each axilla and inferior fold

Some of the influential factors for acute skin reaction are young age and large V-100, which could be measured by simple and cost-efficient methods. According to the literature, CF and radiotherapy are associated with the delivery of higher skin doses to the breast, prostate and other organs during radiation therapy.

On the other hand, in a study by Soleimanifard S et al., mean skin dose in the treatment course

of 50 Gy to the clinical target volume was reported to be 36.65 Gy. Corresponding dose values for patients receiving treatment with and without wedge filter insertion were 35.65 and 37.20 Gy, respectively. According to their findings, the beam angle affected the mean skin dose, while the thickness of the irradiated region and beam entry separation had no effects in this regard.

Since the measured skin dose in the present study was lower than the required amount to prevent tumor recurrence, it is recommended that bolus materials be applied in the course of treatment for post-mastectomy advanced breast radiotherapy. Furthermore, use of wedge filters is necessary to homogenize dose distribution.

Findings of the present study are in line with the current literature, as the calculated skin dose was non-negligible. Additionally, we measured the skin dose in conventional radiotherapy and fractionation, in which the dose value was higher compared to other techniques. To prevent the delivery of additional radiation doses to the skin, application of new techniques is of paramount importance.

5. Conclusion

Although electron contamination dose to the skin tissue seems to be negligible, and the superficial skin dose is not calculated accurately in deep-organ TPSs, results of this study showed an absorption rate of up to 38% of the maximum dose in the skin. MC calculations revealed that contaminant electrons induced approximately 10% (7.3±0.1 Gy of 72 Gy) of the surface dose.

Our findings confirmed MC code as a reliable method for dose calculation and DVH derivation. Moreover, secondary cancer risk estimation conducted by the MC simulation yielded satisfactory results and proposed effectual models. In conclusion, it could be stated that at high doses and dose rates, cell kill exerts a dominant radiobiological effect, while the impact of DNA mutation on cancer induction is negligible. Since we only investigated electron contamination, it is suggested that further studies be performed on electron and neutron contamination.

Aknowledgement: The authors woul like to thank Tabriz University of Medical Sciences research affair for financial supports.

References

1. International Atomic Energy Agency (IAEA safety Report No.47), Radiation Protection in the design of Radiotherapy Facilities, Vienna, 2006;1-145.
2. Hall EJ, Wuu CS. Radiation-induced second cancers: the impact of 3D-CRT and IMRT. Int J Radiat Oncol Biol Phys. 2003; 56:83–8. http://dx.doi.org/10.1016/S0360-3016(03)00073-7
3. Sale KA, Wallace DI, Girod DA, Tsue TT. Radiation-induced malignancy of the head and neck. Otolaryngol Head Neck Surg. 2004; 131:643–5. http://dx.doi.org/10.1016/j.otohns.2004.05.012
4. Swartz D, Terk M, Vashi A, Cesaretti J, Hickson R, Nurani R. Brachytherapy for localized prostate cancer: outcome results with 10 years minimum follow-up. J Urol. 2010: e675. http://dx.doi.org/10.1016/j.juro.2010.02.1596
5. Abdel-Wahab M, Reis IM, Wu J, Duncan R. Second primary cancer risk of radiation therapy after radical prostatectomy for prostate cancer: an analysis of SEER data Urology. 2009; 74:866–71. http://dx.doi.org/10.1016/j.urology.2009.02.085
6. Murray M, Henry A, Hoskin P, Siebert FA, Venselaar J. Second primary cancers after radiation for prostate cancer: A systematic review of the clinical data and impact of treatment technique, Radiother Oncol. 2014;110: 213-228. Doi:10.1016/j.radonc.2013.12.012
7. Schnur JB, Ouellette SC, Dilorenzo TA, Green S, Montgomery GH. A Qualitative Analysis of Acute Skin Toxicity among Breast Cancer Radiotherapy Patients. Psychooncology. 2011; 20(3):260–68. doi: 10.1002/pon.1734.

8. Huang J, Kestin LL, Ye H, Wallace M, Martinez AA, Vicini FA. Analysis of second malignancies after modern radiotherapy versus prostatectomy for localized prostate cancer. Radiother Oncol. 2011; 98:81–6. doi: 10.1016/j.radonc.2010.09.012.
9. Bilge H, Cakir A, Okutan M, Acar H. Surface dose measurements with GafChromic EBT film for 6 and 18 MV photon beams. Phisica Medica. 2009; 52:101-4. doi: 10.1016/j.ejmp.2008.05.001.
10. Butson MJ, Cheung T, Yu PKN. Lepton contamination and photon scatter produced by open field 18 MV X-ray beams in the build-up region. Radiat Meas. 2002; 35:103-7. http://dx.doi.org/10.1016/S1350-4487(01)00278-5
11. Zhu CT, Palta JR. Electron contamination in 8 and 18 MV photon beams. Med Phys. 1998; 25:12-9. DOI 10.1118/1.598169
12. Biggs PJ, Ling CC. Improving the buildup and depth-dose characteristics of high energy photon beams by using electron filters. Med Phys. 1979; 6:296-301. DOI:10.1118/1.598169
13. Mackie TR, Scrimger JR. Contamination of a 15-MV photon beam by electrons and scattered photons. Radiology. 1982; 144: 403–9. DOI:10.1148/radiology.144.2.6806853
14. Beauvais H, Bridier A, Dutreix A. Characteristics of contamination electrons in high energy photon beams. Radiother. Oncol. 1993; 29: 308–16. Doi:10.1016/0167-8140(93)90149-3
15. Attix FH, Lopez F, Owolabi S, Paliwal BR. Electron contamination in 60Co gamma-ray beams. Med Phys. 1983; 10: 301–6. DOI:10.1118/1.595305
16. Rustgi SN, Gromadzki ZC, Ling CC, Yorke ED. Contaminant electrons in the build-up region of a 4 MV photon beam. Phys Med Biol. 1983; 28:659–65. PMID:6410419
17. Yorke ED, Ling CC, Rustgi S. Air-generated electron contamination of 4 and 10 MV photon beams: A comparison of theory and experiment. Phys Med Biol. 1985; 30:1305–14.
18. Trott KR, Kummermehr J. Radiation effects in skin; in Scherer E, Streffer C, Trott KR (eds): Radiopathology of Organs and Tissues. Berlin, Springer. 1991; pp 33–66.
19. Lawenda BD, et al. Permanent alopecia after cranial irradiation: Dose-response relationship. Int J Radiat Oncol Biol Phys. 2004; 60:879–887. http://dx.doi.org/10.1016/j.ijrobp.2004.04.031
20. Schneider U, Zwahlen D, Ross D et al. Estimation of radiation induced cancer from three-dimensional dose distributions: Concept of organ equivalent dose. Int J Radiat Oncol Biol Phys. 2005; 61(5):1510-5. DOI: 10.1016/j.ijrobp.2004.12.040
21. Hall EJ, Wuu CS. Radiation-induced second cancers: the impact of 3D-CRT and IMRT. Int J Radiat Oncol Biol Phys. 2003; 56(1):83-8. PMID: 12694826
22. International Commission on Radiological Protection. The 2007 recommendations of the International Commission on Radiological Protection, ICRP No. 103, Ann. ICRP 37, 2007. doi:10.1016/S1507-1367(04)71038-X
23. Kukołowicz P. Clinical aspects of normal tissue complication probability. Reports Prac Oncol Radiother. 2004; 9:261-7.
24. Harrison RM, The estimation of second cancer risk following radiotherapy: a discussion of two models. Biomed Imag and Intervention Jour. 2007;3(2): e54. Doi:10.1.1.651.9743
25. Emami B, Lyman J, Brown A, et al. Tolerance of normal tissue to therapeutic radiation. Int J Radiat Oncol Biol Phys. 1991; 21:109 –22. Doi:10.1016/0360-3016(91)90171-Y
26. Zaider M, Amols H I. Practical considerations in using calculated healthy –tissue complication probabilities for treatment- plan optimization. Int. J. Radiat Oncol Biol Phys. 1999; 44: 439-47. http://dx.doi.org/10.1016/S0360-3016(99)00014-0
27. Zwicker RD, Andrew Wu A, Curran BH, Sternick ES. Electron contamination due to Lucite in a 45- MV photon beam. Med Phys. 1984; 11:534
28. Li XA,Rogers DWO. Reducing electron contamination for photon beam- quality specification. Med Phys. 1994; 21:791. DOI:10.1118/1.597395
29. Mallikarjuna RB, Prasad SG, Parthasaradhi K, Lee Y, Ruparel R, Garces R. Investigations on the near surface dose for three 10- MV x- ray beam accelerators with emphasis on the reduction of electron contamination. Med Phys. 1988; 15:246. DOI:10.1118/1.596256
30. Smit C, du Plessis F. SU-E-T-238: Deriving Electron Contamination Spectra From Pure and Clinical Photon Beams. Med Phys. 2015; 42:3387.
31. Harper NR, Metcalfe PE, Hoban PW, Round WH . Electron contamination in 4 MV and 10 MV radiotherapy x-ray beam. Australas Phys Eng Sci Med. 1991;14(3):141-5. PMID:1953499
32. Nilsson B, Brahme A. Electron contamination from photon beam collimators. Radiother and Oncol. 1986; 5(3):235-44.
33. Mesbahi A. A Monte Carlo study on neutron and electron contamination of an unflattened 18-MV photon beam. Appl Radiat Isotopes. 2009; 67(1):55-60. doi:10.1016/S0167-8140(86)80053-6

34. Sjögren R, Karlsson M. Influence of electron contamination on in vivo surface dosimetry for high-energy photon beams. Med Phys. 1998; 25:916. DOI:10.1118/1.598270
35. Medina AL, Lopez A, Teijeiro A et al. Characterization of electron contamination in megavoltage photon beams. Med Phys. 2005; 32(5):1281-92. DOI:10.1118/1.1895793
36. Allahverdi1 M, Zabihzadeh M, Ay MR. Monte Carlo estimation of electron contamination in an 18 MV clinical photon beam. Iran J Radiat Res. 2011; 9(1): 15-28. URL: http://ijrr.com/article-1-728-en.html
37. Dasu A, Toma-Dasu I, Olofsson J, Karlsson M. The use of risk estimation models for the induction of secondary cancers following radiotherapy. Acta Oncol.2005;44(4):339-47. DOI:10.1080/02841860510029833
38. Martin JB, Tsang C, Peter Y, Peter EM. Evaluation of a radiotherapy electron contamination deflecting system. Rad Meas. 2000; 32:101-4. http://dx.doi.org/10.1016/S1350-4487(99)00267-X
39. oral Comparison of Monte Carlo simulation and TPS calculation of radiosurgery treatment DVHS by means of TCP and NTCP parameters. Radiotherapy and Oncology. 2003; 68: S19. doi:10.1016/S0167-8140(03)80054-3
40. Ojala J, Hyödynmaa S. MC-BASED VERIFICATION OF ABSORBED DOSE DISTRIBUTIONS IN THE LUNG CALCULATED BY TWO ELECTRON BEAM ALGORITHMS. Radiotherapy and Oncology. 2011: 99: S177. doi:10.1016/S0167-8140(11)70561-8
41. Rudat V, Nour A, Ghaida SA, Alaradi A. Impact of hypofractionation and tangential beam IMRT on the acute skin reaction in adjuvant breast cancer radiotherapy. Radiotherapy and Oncology 2016. doi: 10.1186/s13014-016-0674-y. doi: 10.1186/s13014-016-0674-y.